Available online at www.sciencedirect.com

SCIENCE DIRECT®

Applied Clay Science 29 (2005) 155–171

Applied CLAY Science

www.elsevier.com/locate/clay

Modeling of transport and reaction in an engineered barrier for radioactive waste confinement

G. Montes-H[a,*], B. Fritz[a], A. Clement[a], N. Michau[b]

[a] *UMR 7517 ULP-CNRS, CGS, 1 rue Blessig, F-67084 Strasbourg, France*
[b] *ANDRA, 1/7 rue Jean Monnet, 92298 Châtenay-Malabry Cedex, France*

Received 15 March 2004; received in revised form 20 December 2004; accepted 11 January 2005
Available online 3 March 2005

Abstract

Bentonites have been proposed as buffer materials for barriers in geological disposal systems for radioactive waste. In these conditions the bentonite barriers may be submitted to changes of humidity, temperature variation, fluid interaction, mass transport, etc. This could modify the physico-chemical performance of the barrier, mainly on the interface with the steel container and with the geological barrier. The engineered barrier development necessitates thus the study of the physico-chemical stability of its mineral constituents as a function of time under the conditions of the repository in the long term. The aim of this paper is to simulate the chemical transformations of the engineered barrier and chemical-elements diffusion impact resulting from the temperature increase (disintegration reactions of wastes), the presence of fluids coming from the geological barrier, and from the liberation of iron (degradation of the containers). The current study was based on the laboratory experiments and mineral characterization achieved by LEM and GREGU research laboratories.

The simulations to predict the chemical transformations of argillaceous barrier (MX80 bentonite) and chemical-elements diffusion impact (water-saturated medium) were carried out by using a thermo-kinetic hydrochemical code (KIRMAT: Kinetic Reactions and Mass Transport). This code considers a 1D multisolute mass transport system. Here, all simulations were made in reducing initial conditions ($P_{O_2} \cong 0$; $E_h = -200$ mV) and the reaction temperature was considered as constant at 100 °C during 1000 years.

The results show that the more significant chemicals transformations were (1) the Na/Ca–montmorillonite-to-Ca–montmorillonite conversion, (2) the montmorillonite-to-chlorite conversion and (3) the dissolution/precipitation of accessory minerals. The first chemical transformation represents about 22% in the worst case, i.e., near of the engineered barrier interfaces while the second chemical transformation only represents about 3% (near the container), i.e., a high concentration of iron favours the chlorite–FeAl precipitation. Concerning the dissolution/precipitation of accessory minerals, in general, it was observed that the quartz, microcline and albite were re-precipitated in the system; the calcite and biotite were partially dissolved, and the pyrite was kept inactive.

Keywords: Engineered barrier; MX80 bentonite; Radioactive waste; Modelling; KIRMAT code; Chemical transformations; Mass transport

* Corresponding author. Fax: +33 390240402.
E-mail addresses: montes@illite.u-strasbg.fr, german_montes@hotmail.com (G. Montes-H).

0169-1317/$ - see front matter © 2005 Elsevier B.V. All rights reserved.
doi:10.1016/j.clay.2005.01.004

1. Introduction

A particular radioactive waste disposal design proposes to store waste in deep geological layers of impervious clay. Vitrified waste is laid in canisters in the middle of a gallery dug in the clay formations. In order to protect canisters from water intrusion and to eventually trap released radioelements, waste-forms will be isolated from the surrounding geological media by two barriers: (a) the steel canister and (b) an engineered backfill barrier system. This backfill barrier will be essentially composed of compacted clay blocks because of the hydro-dynamic and surface properties of clay materials. In France, nowadays, the reference backfill material is a commercial clay referred to as MX80 bentonite (bentonite of Wyoming). This commercial "clay" contains montmorillonite (80%), quartz (6%), K-feldspars (2%), plagioclases (4%), carbonates (4%), mica (3%) and other minerals (1%) (Sauzeat et al., 2001). The bulk sample is composed by 86.1% of particles in a size range below 2 μm, 8.8% in the 2–50-μm range and 5.1% of sizes over 50 μm (Neaman et al., 2003).

One major question is: what will be the long-term physical and chemical evolution of the engineered barrier? At the present time, several approaches have been reported in the literature, considering the different physico-chemical phenomena such as temperature variation, fluid circulation, contaminant migration, hydration/dehydration phenomena, mechanical deformation, physico-chemical alteration, etc. Unfortunately, the coupling of all phenomena in the same numerical model still remains difficult (Poinssot and Toulhoat, 1998; Collin et al., 2002; Gens et al., 2002; Keijzer et al., 1999; Malisis and Shackelford, 2002; Ulm et al., 2002; Le Gallo et al., 1998; Savage et al., 2002; Hökmark et al., 1997; Kälvenius and Ekberg, 2003).

The main purpose of this paper is to simulate the chemical transformations of the engineered barrier and chemical-elements diffusion impact resulting from the temperature increase (disintegration reactions of wastes), the presence of fluids coming from the geological barrier, and from the liberation of iron (degradation of the containers). For that, a thermo-kinetic hydrochemical code (KIRMAT: Kinetic Reactions and Mass Transport) was used (Gérard et al., 1998). This code considers a 1D multisolute mass transport system and is based on the steady-state or stationary-state properties of the thermo-kinetic Eulerian reactive transport mass balance equations. Here, all simulations were made in reducing initial conditions ($P_{O_2} \cong 0$; $E_h = -200$ mV) and the reaction temperature was considered as constant at 100 °C during 1000 years (see Fig. 1).

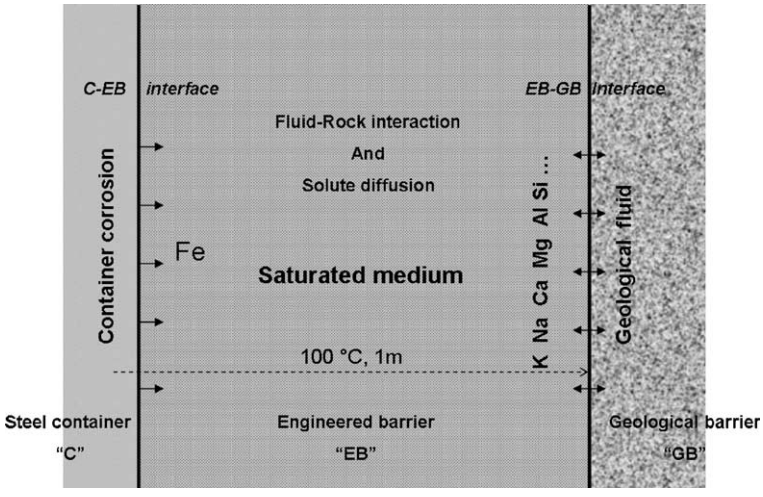

Fig. 1. Schematic representation of fluid–rock reaction and solute diffusion in an engineered barrier for radioactive waste confinement.

2. Model description

The Eulerian thermo-kinetic hydrochemical code KIRMAT (Gérard et al., 1998) has been developed from the single reaction path model KINDIS (Madé et al., 1994), by keeping all its geochemical formulation and its numerical method to solve chemical equations.

The thermo-kinetic geochemical code KINDIS was developed from the purely thermodynamic code DISSOL (Fritz, 1975, 1981; Fritz and Tardy, 1976), which in turn originated from PATH1 (Helgeson et al., 1970). Theoretical kinetic rate laws for mineral dissolution and precipitation based on the Transition State Theory (TST) have been implemented in DISSOL. These geochemical codes have been intensively numerically tested and used in published studies on hydrothermal, diagenetic, and weathering processes (e.g., Nöack et al., 1993; Bertrand et al., 1994).

In KINDIS, the irreversible kinetic driving force is explicitly calculated and the sequence of partial equilibrium state is calculated from second-order Taylor series expansion.

In KIRMAT, solute transport is added to kinetic dissolution and/or precipitation reactions. A chemically controlled time step (noted Δt_c) allows to preserve accuracy of the calculations. Its value is chosen inversely proportional to the largest of the first derivative variations among all the solute concentrations, and is controlled by setting the θ parameter (inversely proportional to Δt_c). The set of the partial differential equations is integrated along one direction with the classical finite difference approximation method. An explicit scheme and a one-step algorithm are used to solve simultaneously the chemical (from KINDIS) and the conservative transport mass balance equations. A classical mixing cell scheme, the explicit-backward discretization, is computed for a numerical validation study.

3. Methodology

3.1. General considerations

All simulations presented here were performed using version 1.6 of the thermo-kinetic hydrochemical code KIRMAT (Gérard et al., 1998). The main interest was to simulate the chemical transformations of engineered barrier (hydrolysis reactions) and chemical-elements diffusion impact (mainly Fe, K, Ca, Na, Mg, etc.) in the saturated porous media under conditions of the repository. The following aspects were considered to simplify the modelling system.

3.1.1. Geochemical transformations in a fluid-saturated medium

A recent study showed that a bentonite barrier is fully water-saturated within approximately 3–4 years after deposition (Hökmark, 2004). Then, it was supposed that the interface contact "engineered barrier-geological medium" operates as a permeable membrane only to the water during the hydration phase of the engineered barrier. In this case, the chemical species contained in the geological fluid will only be adsorbed (or retarded) in the first few centimeters of the engineered barrier. These comments allow the assumption that initially the engineered barrier is saturated with a fluid of low concentration. In the present study, the engineered barrier is initially saturated with pure water or with a fluid of low concentration.

3.1.2. Solute diffusion

In the water-saturated engineered barrier of bentonite, the interstitial fluid is almost static because of the very low permeability in the medium. In these conditions, the convection transport can be negligible. Then, the significant transport phenomenon through the engineered barrier is uniquely the diffusion of chemical elements, mainly iron diffusion toward the geological medium and K, Ca, Na, Si, etc. diffusion toward the metallic container.

3.1.3. Reducing conditions

Following the closing of the repository system, the hydrolysis reactions of the mineral constituents "of the engineered barrier" take place in reducing conditions ($P_{O_2} \cong 0$; $E_h = -200$ mV) because the oxygen is consumed rapidly.

3.1.4. Container corrosion

In the KIRMAT code, it is difficult to take the container corrosion directly into account. At the present time, two possibilities are considered:

– A significant concentration of total iron (0.001 mol/kg H_2O) in the boundaries of container. That

is, this possibility does not consider the container corrosion rate. Here, the total concentration was taken arbitrarily constant during 1000 years of simulation.

– The second possibility allows to consider the container corrosion as a dissolution reaction in reducing conditions:

$$Fe^0 + 2H_2O \Leftrightarrow Fe^{++} + 2OH^- + H_2 \uparrow$$

This perturbation into the system was simulated by a standard kinetic equation of mineral dissolution where the rate constant of iron dissolution was estimated considering a linear rate of corrosion of 5 μm/year during 100 years. The rate constant of iron dissolution was then estimated using the following formula:

$$k_{d_{Fe}} = \frac{v_{\text{corrosion}}.\rho}{\overline{M}}, \left[\ \text{mol}\ /\left(\text{m}^2\ \text{year}\ \right)\right] \quad (1)$$

with $v_{\text{corrosion}}$ as the rate linear corrosion, ρ as the specific (grain) density, and $\overline{M}$ as the molar mass of iron.

3.1.5. Initial state of the engineered barrier

Two scenarios were taken into account: in the first scenario, the engineered barrier is initially in disequilibrium with the interacting solution (pure water). In this case, the system is "very reactive." In contrast, in the second scenario, the stationary state of the system was reached by a previous simulation in closed system, i.e., without mass transport. Here, the interacting fluid is slightly charged in Na^+, H_4SiO_4, and K^+.

3.2. Conceptual system

The system modelled herein was considered to consist of a 1-m-thick zone of water-saturated engineered barrier "of bentonite clay." This non-equilibrated or stationary-state system was placed in contact with a geological fluid on one side, which was then allowed to diffuse into the barrier, while the other was kept in contact with iron-charged water (0.001 mol/kg H_2O) or with a source of metallic iron. This configuration represents the contact of engineered barrier with geological medium and with container in a geological disposal facility for radioactive wastes (Fig. 1).

A grid spacing of 5 cm was used for all the calculations reported, i.e., the thick zone of engineered barrier was divided into 20 grids.

Several simulations were carried out in order to study the montmorillonite-to-illite, montmorillonite-to-chlorite and montmorillonite-to-zeolite conversions and to estimate the chemical-elements diffusion impact in the bentonite barrier.

(a) A significant concentration of total iron (0.001 mol/kg H_2O) in the boundaries of container and the engineered barrier in initial disequilibrium with the interacting solution.

Case 1. A geological fluid lowly concentrated with K (5.4×10^{-2} mol/kg H_2O); $D_{\text{eff}}=10^{-11}$ m^2/s

Case 2. A geological fluid lowly concentrated with K (5.4×10^{-2} mol/kg H_2O); $D_{\text{eff}}=10^{-10}$ m^2/s

Case 3. A geological fluid concentrated with K (5.4×10^{-1} mol/kg H_2O), $D_{\text{eff}}=10^{-11}$ m^2/s

Case 4. A geological fluid concentrated with K (5.4×10^{-1} mol/kg H_2O), $D_{\text{eff}}=10^{-10}$ m^2/s

Case 5. A representative geological fluid of the French Callovo-Oxfordian formation (see Table 4); $D_{\text{eff}}=10^{-11}$ m^2/s

(b) A significant concentration of total iron (0.001 mol/kg H_2O) in the boundaries of container and the engineered barrier in initial stationary state with the interacting solution.

Case 6. A representative geological fluid of the French Callovo-Oxfordian formation (see Table 4); $D_{\text{eff}}=10^{-11}$ m^2/s

(c) The iron dissolution (v_c=5 μm/year) in the boundaries of container and the engineered barrier in initial stationary state with the interaction solution.

Case 7. A representative geological fluid of French Callovo-Oxfordian formation (see Table 4); $D_{\text{eff}}=10^{-11}$ m^2/s.

4. Input data

4.1. Primary minerals

The MX80 bentonite has been widely studied by Sauzeat et al. (2001), Montes-H (2002), Montes-H et al. (2003, 2004), Neaman et al. (2003), Hökmark et al. (1997), and others. This commercial clay mineral

Table 1
Mineral composition of MX80 bentonite (Sauzeat et al., 2001) and thermodynamic equilibrium constants used in KIRMAT simulations

Mineral	[%]	Chemical formula	Log (K_m) (100 °C)
Pyrite	0.3–0.6	FeS_2	−67.89[a]
Calcite	0.96–1.5	$CaCO_3$	−9.39[a]
Quartz	6–7	SiO_2	−3.095[a]
Microcline	1–2	$KAlSi_3O_8$	−18.104[a]
Albite	3–4	$NaAlSi_3O_8$	−16.037[a]
Biotite	2–3	$K(Fe_{1.5}Mg_{1.5})[Si_3AlO_{10}](OH)_2$	5.910[a]
Na/Ca–montmorillonite	80–84	$[Si_{3.98}Al_{0.02}O_{10}](OH)_2$ $(Al_{1.55}Mg_{0.28}Fe^{III}_{0.09}Fe^{II}_{0.08})$ $(Na_{0.18}Ca_{0.10})$	−28.455[b]

[a] Database of KIRMAT code.
[b] The sum of polyhedral contributions (Chermak and Rimstidt, 1989, 1990).

contains about 85% of Na/Ca–montmorillonite and 15% of accessory minerals (see Table 1). In the present study, the minerals contained in the MX80 bentonite were considered as primary minerals or as reactants of any possible mineral dissolution (or chemical transformation). In the KIRMAT simulations, the dissolution of primary minerals was treated with a kinetic option. In contrast, their precipitation was considered with a thermodynamic equilibrium option.

4.2. Secondary minerals

The secondary minerals or neo-formed mineral phases were chosen following the conclusions of the laboratory experiments conducted at 80 and 300 °C in the presence of metallic iron (Guillaume, 2002). Table 2 presents the secondary minerals considered in the KIRMAT simulations. The secondary mineral precipitation (or neo-formation) was treated with a thermodynamic option (i.e., equilibrium condition for precipitation).

4.3. Fluid initial composition

The engineered barrier was considered as a saturated medium, initially saturated with pure water or with a fluid slightly charged in Na^+, H_4SiO_4 and K^+. In contrast, the geological fluid was a representa-

Table 2
Secondary minerals and the thermodynamic equilibrium constants used in KIRMAT simulations

Mineral	Chemical formula	Log (K_m) (100 °C)
Vermiculite MgFe2	$[(Si_{3.67}Al_{0.33}O_{10})(OH)_2](Al_{0.33}Fe^{II}_{1.15}Mg_{1.52})$	−5.14[a]
Saponite Fe(II)	$[(Si_{3.67}Al_{0.33}O_{10})(OH)_2](Fe^{II}_3)Na_{0.33}$	−2.05[a]
Saponite MgFe(II)	$[(Si_{3.5}Al_{0.5}O_{10})(OH)_2](Al_{0.25}Fe^{II}_{1.25}Mg_{1.5})Ca_{0.05}Na_{0.15}$	−2.11[a]
Montmorillonite–Na	$[(Si_{3.96}Al_{0.04}O_{10})(OH)_2](Al_{1.52}\ Fe^{III}_{0.18}Mg_{0.27})Na_{0.4}$	−28.84[a]
Montmorillonite–Ca	$[(Si_{3.96}Al_{0.04}O_{10})(OH)_2](Al_{1.52}\ Fe^{III}_{0.18}Mg_{0.27})Ca_{0.2}$	−29.23[a]
Phillipsite Na	$[Si_{10}Al_6O_{32}]Na_5Ca_{0.5} \cdot 12H_2O$	−72.05[a]
Laumonite	$[SiAl_2O_8]Ca \cdot 4H_2O$	−26.38[b]
Chabazite Na	$[Si_8Al_4O_{24}]Na_{3.5}Ca_{0.25} \cdot 13H_2O$	−51.26[a]
Chlorite FeAl	$[Si_2Al_2O_{10}(OH)_2](Fe^{II}Al_2)(Fe^{II}_3)(OH)_6$	−55.57[a]
Chlorite MgAl	$[Si_2Al_2O_{10}(OH)_2](MgAl_2)(Mg_3)(OH)_6$	−31.23[a]
Illite	$[(Si_{3.5}Al_{0.5}O_{10})(OH)_2](Al_{1.8}Mg_{0.25})K_{0.6}$	−35.23[b]
Goethite	$FeO(OH)$	8.82[b]
Siderite	$FeCO_3$	−11.95[b]
Magnetite	Fe_3O_4	22.65[b]
Anhydrite	$CaSO_4$	−5.36[b]
Gypsum	$CaSO_4 \cdot 2H_2O$	−5.010[b]
Thenardite	Na_2SO_4	−0.640[b]
Jarosite	$KF^{III}_3(SO_4)_2(OH)_6$	20.84[b]

[a] The sum of polyhedral contributions (Chermak and Rimstidt, 1989, 1990).
[b] Database of KINDISP model.

tive geological fluid of the French Callovo-Oxfordian formation (see Table 3).

4.4. Temperature of reaction

In the KIRMAT code, it is not possible to take into account the temperature gradient as a function of time produced by the disintegration reactions of radioactive wastes. However, it is possible to take into account any temperature between 0 and 300 °C. The confinement barrier is subjected to temperature variations, (>70 °C and sometimes>100 °C) (Collin et al., 2002). In the present study, a constant temperature of 100 °C during 1000 years was assumed.

4.5. Initial pH and P_{CO_2}

$P_{CO_2}$was initially fixed at 3.16 10^{-4} bar. Knowing that the alkaline reserve is close to zero for the pure water, the initial pH was calculated at 5.89 considering a temperature of 100 °C.

4.6. Water–rock ratio

The initial physical porosity of MX80 bentonite was estimated at 30% (Sauzeat et al., 2001). Assuming that the engineered barrier is initially saturated with pure water and knowing that the KIRMAT code is based on 1 kg of water (i.e., approximately 1000 cm^3 "V_{water}"); it was very easy to estimate the volume rock involved in the interaction (approximately 2333 cm^3). This value and the mineral volume fraction allow the calculation of the initial volume of each primary mineral in the system.

Table 3
Chemical composition, pH, and E_h of a representative geological fluid from Callovo-Oxfordian formation (Jacquot, 2002)

Chemical parameters	Value	Observation
E_h [mV]	−185	SO_4/pyrite equilibrium
pH	7.30	electroneutrality condition
Na [mol/kg H_2O]	4.17×10^{-2}	Na–Ca exchange
K [mol/kg H_2O]	5.40×10^{-3}	K–Ca exchange
Ca [mol/kg H_2O]	9.74×10^{-3}	equilibrium with calcite
Mg [mol/kg H_2O]	7.68×10^{-3}	Na–Mg exchange
SiO_{2aq} [mol/kg H_2O]	9.44×10^{-5}	equilibrium with quartz
Cl [mol/kg H_2O]	7.19×10^{-2}	calculated by lixivation
SO_4 [mol/kg H_2O]	4.40×10^{-3}	P_{CO_2}=3.09×10^{-3} condition
Al [mol/kg H_2O]	9.26×10^{-9}	equilibrium with illite
Fe [mol/kg H_2O]	6.44×10^{-5}	equilibrium with daphnite
C_T (inorganic) [mol/kg H_2O]	1.44×10^{-3}	equilibrium with dolomite
P_{CO_2} [atm]	3.09×10^{-3}	–

4.7. Thermodynamic equilibrium constants

The KIRMAT code is based on hydrolysis reactions where the major aqueous species are mainly H_4SiO_4, $Al(OH)_4^-$, CO_3^-, SO_4^-, Na^+, K^+, Ca^{++}, Mg^{++}, Fe^{++}, Fe^{+++}, H_3O^+, and H_2O. The thermodynamic equilibrium constants of hydrolysis reactions used in KIRMAT simulations at 100 °C are presented in Tables 1 and 2.

4.8. Kinetic data

The simplified equation used to simulate the dissolution rate of a mineral m in KIRMAT code may be written as

$$v_{dm}^{s} = k_{dm}^{pH} S_m^{eff} a_{H^+}^{n} \left(1 - \frac{Q_m}{K_m}\right) \quad (2)$$

where k_{dm}^{pH} is the constant of the apparent dissolution rate intrinsic to mineral m at a given pH [mol/m^2/year]; S_m^{eff} is the effective or reactive surface area (as a function of the number of actives sites) at the mineral/aqueous solution interface [m^2/kg H_2O]; $a_{H^+}^{n}$ is the activity of the H^+ ions in the aqueous solution, where n is a real exponent with a generally positive value in acid solutions, zero in neutral solutions and negative in basic solutions; and $(1-Q_m/K_m)$ is the saturation index of mineral m in a aqueous solution, where Q_m is the ionic activity product and K_m is the thermodynamic equilibrium constant known for the given temperature and pressure conditions.

The intrinsic constant of the mineral dissolution (k_{dm}^{pH}) is a function of the temperature which can be described by the Arrhenius law:

$$k_{dm}^{pH} = A_m \exp\left(\frac{-E_{am}}{RT}\right) \quad (3)$$

with A_m being the frequency factor and E_{am} the activation energy of mineral dissolution reaction [J mol^{-1}].

The k_{dm}^{pH} data used in the current study were taken from studies by Jacquot (2000) and Kluska and Fritz (2001). These values are summarized in the Table 4.

Table 4
The kinetic data used in the KIRMAT simulations

Mineral	$S_m^{eff\dagger}$ [m^2/kg H_2O]	k_{dm}^{pH} [mol/m^2.year]			pH limit	
		$k^{H\dagger}$	$k^{H2O\dagger}$	$k^{OH\dagger}$	A-to-N	N-to-B
Pyrite	2.19	1.88×10^{-18}	1.88×10^{-18}	1.88×10^{-18}	–	–
Calcite	6.76	7.93×10^{6}	8.69×10^{2}	8.69×10^{2}	4.4	8.3
Quartz	49.22	4.5×10^{-3}	1.7×10^{-3}	3.18×10^{-6}	2	6.5
Microcline	7.46	1.40	7.89×10^{-3}	5.97×10^{-6}	4.5	7.8
Albite	24.42	1.40	7.89×10^{-3}	5.97×10^{-6}	4.5	7.8
Biotite	19.48	1.34×10^{-3}	1.89×10^{-5}	5.45×10^{-7}	5	7
Montmorillonite	590.4	1.34×10^{-3}	1.89×10^{-5}	5.45×10^{-7}	5	7

k^H: constant of the dissolution rate in an acid medium.
k^{H2O}: constant of the dissolution rate in a neutral medium, independent of the pH.
k^{OH}: constant of the dissolution rate in a basic medium.
S_m^{eff}: reactive surface area.
A: acid; N: neutral; B: basic.
† Kinetic data (after Jacquot, 2002; Kluska and Fritz, 2001).

Conversely, the effective or reactive surface area (S_m^{eff}) could be defined as a percentage of the total mineral surface area, generally between 50% and 90% (White and Peterson, 1990). Recently, the atomic force microscopic experiments showed that only 8–14% of the total mineral surface area participate as reactive surface area (S_m^{eff}) in the dissolution of several silicates (Nagy et al., 1999; Tournassat et al., 2003). It is still difficult to estimate with precision the reactive surface area of silicates and phyllosilicates. Granular studies show that a bulk sample of MX80 bentonite is composed by 86.1% of particles <2 μm in size, 8.8% in the 2–50-μm range and 5.1% >50 μm (Neaman et al., 2003). In the present study, it was supposed (which is not really true) that the MX80 bentonite was composed of particles of 2 μm in size. This consideration simplified the calculation of the total mineral surface area (S_m^T) for each primary mineral. Finally, it was also assumed that only 10% of the total mineral surface area participated as reactive surface area ($S_m^{eff}=0.1S_m^T$). Evidently, these assumptions are rough, but this estimation of reactive surface area of mineral phases is still discussed in the literature.

The kinetic data (k_{dm}^{pH}, S_m^{eff}) used in the KIRMAT simulations are presented in Table 4.

4.9. Diffusion coefficients

The transport of solutes into the clay barrier was considered to be a pure diffusion process in a saturated medium. The initial effective diffusion coefficients tested in the simulations were 10^{-11} and 10^{-10} m^2/s. These values were selected based on published data for compacted MX80 (Lehikoinen et al., 1996). The KIRMAT code uses the same value for all chemical species and considers a constant molecular diffusion.

5. Results and discussion

5.1. General comments

The dominant presence of Na/Ca–montmorillonite in the MX80 bentonite could cause it to perform exceptionally well as an engineered barrier for a radioactive waste repository because of its swelling–shrinkage property (see Fig. 2). ESEM observations showed, for example, that an argillaceous rock containing dominant montmorillonite (swelling clay) has the capacity of cracks closing (see Fig. 3) while an argillaceous rock containing dominant non-swelling clays presents uniquely a progressive cracking (see Fig. 4) after hydration/dehydration cycles (Montes-H et al., 2004).

Knowing that the protection performance for an engineered barrier of bentonite is directly linked on the montmorillonite swelling property, their development necessitates the investigation on the chemical transformations of montmorillonite under repository conditions as a function of time. In this case, the

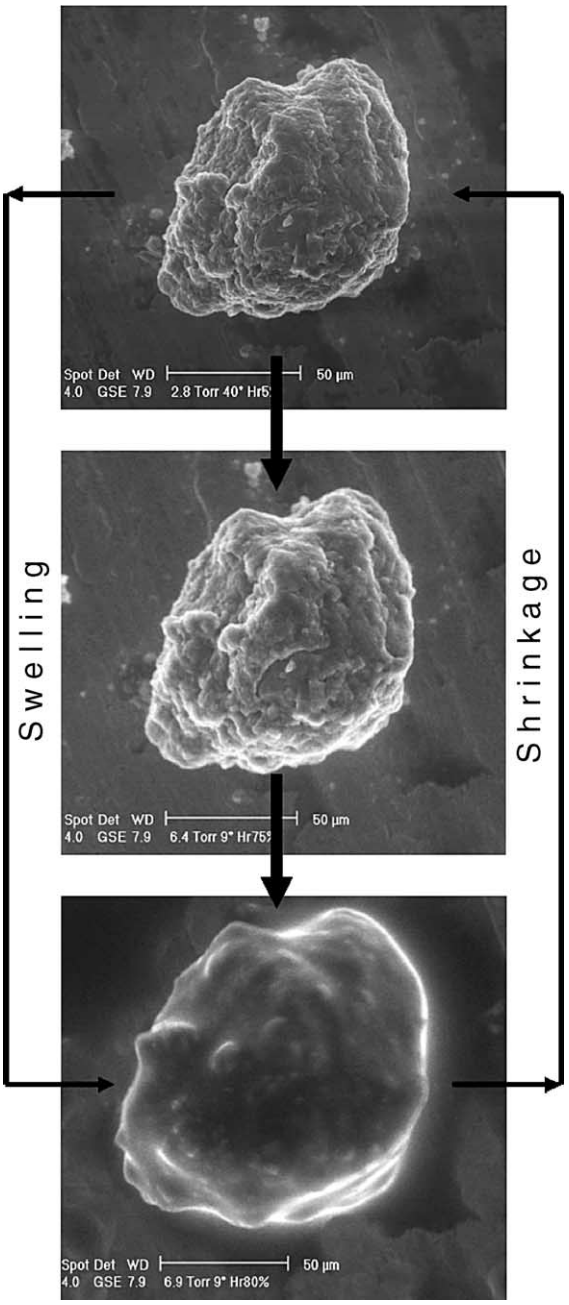

Fig. 2. Swelling–shrinkage property of MX80 bentonite (Montes-H, 2002).

reaction-transport modeling is a precious tool. In the following paragraphs, the montmorillonite-to-illite, montmorillonite-to-chlorite and montmorillonite-to-zeolite conversions are described.

5.1.1. Montmorillonite-to-illite conversion

The Na/Ca–montmorillonite-to-illite conversion is a potential chemical process for a bentonite barrier in the radioactive waste repository because of high-concentration potassium in the geological fluid (Hökmark et al., 1997; Guillaume, 2002).

Fig. 5 shows the saturation index evolution of the illite in the engineered barrier; here, the possibility of illite precipitation takes place only in the first 5 cm because the saturation index (Q/K) is equal to 1. However, the illite production could be negligible, but, this phenomenon is effectively more significant when the potassium concentration increases in the interacting fluid.

In conclusion, it is reasonable to predict that the montmorillonite-to-illite conversion depends on the reaction temperature and on the geological fluid concentration, particularly on the potassium concentration. In the present study, this chemical process is not significant after 1000 years of reaction and transport.

5.1.2. Montmorillonite-to-chlorite conversion

The montmorillonite-to-chlorite conversion is also a potential chemical process for bentonite barrier in the radioactive waste repository because of a significant iron concentration in the geological fluid (Table 3) and also because of the iron liberation by the container corrosion. KIRMAT simulation (case 5) showed that the high iron concentration favours the Na/Ca–montmorillonite dissolution. In fact, the Na/Ca–montmorillonite dissolution is calculated to be more significant near the iron container (see Fig. 6). In addition, the high iron concentration also favours the montmorillonite-to-chlorite conversion. For example, this chemical process constitutes about 10% of the Na/Ca–montmorillonite dissolution near the container then this value decreases until about 8% in the bentonite barrier (Fig. 6). It is clear that a montmorillonite-to-chlorite conversion will limit the swelling property of a bentonite barrier. Fortunately, this chemical transformation only represents about 3% of the total Na/Ca–montmorillonite contained in the bentonite barrier. In this study, only two chlorites at 14 Å were tested (see Table 2), knowing that these chlorites are typically neoformed at high temperature, i.e., a temperature >100 °C (Guillaume, 2002).

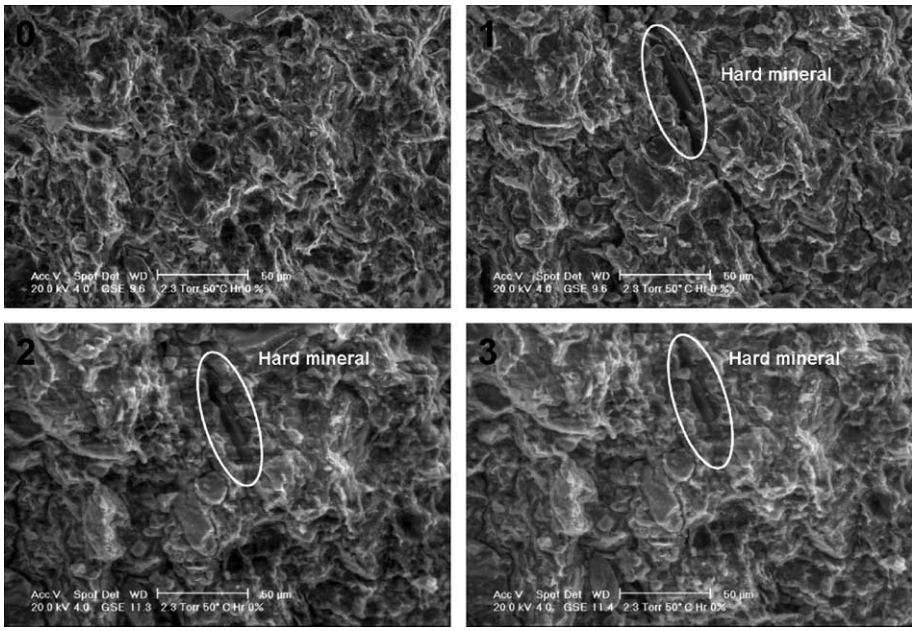

Fig. 3. Partial closing of the cracks for an argillaceous rock (argillite) containing swelling clays after hydration/dehydration cycles in the ESEM (Montes-H et al., 2004). (0) Initial conditions; (1) first cycle; (2) second cycle; (3) third cycle.

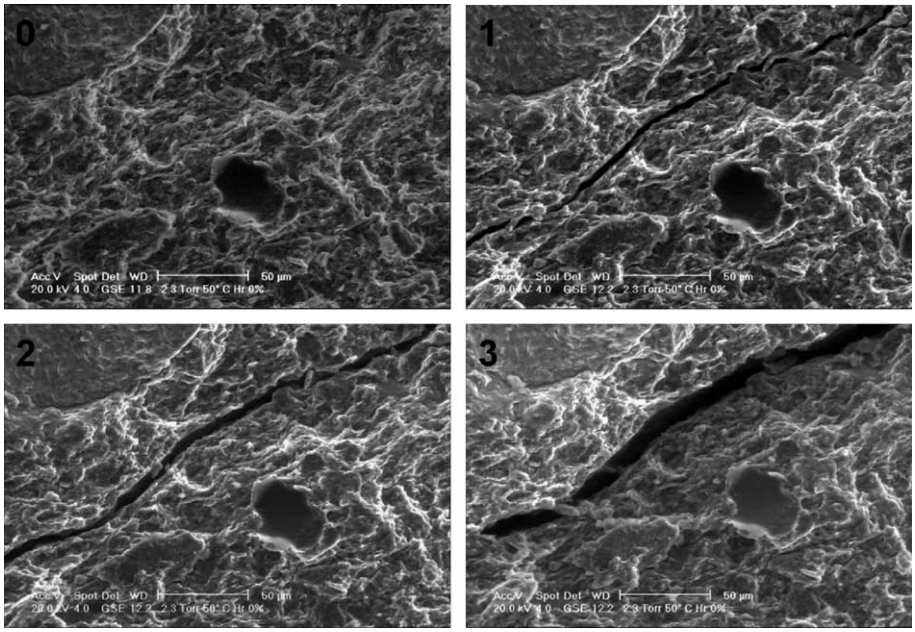

Fig. 4. Progressive cracking for an argillaceous rock (argillite) containing non-swelling clays after hydration/dehydration cycles in the ESEM (Montes-H et al., 2004). (0) Initial conditions; (1) first cycle; (2) second cycle; (3) third cycle.

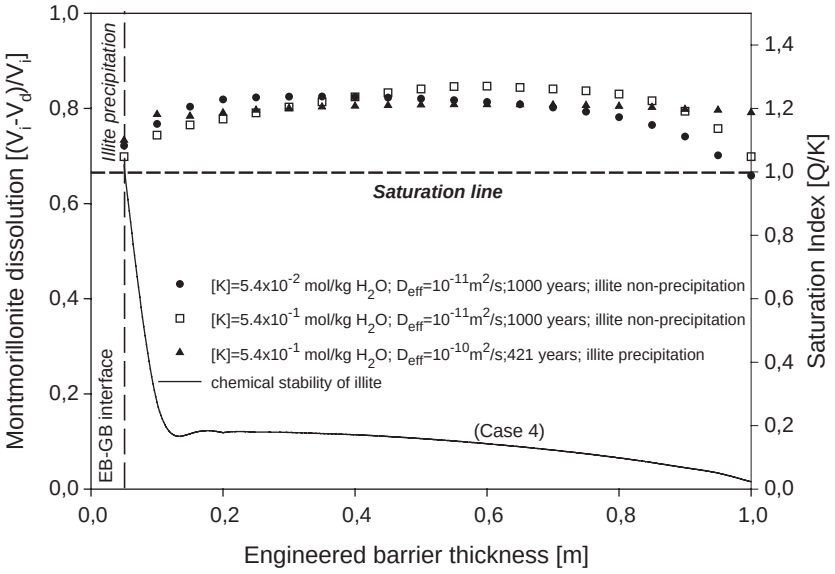

Fig. 5. Montmorillonite volume fraction after 1000 years of reaction and transport, and representation of illite precipitation in the MX80-bentonite barrier. V=Volume; i=initial and d=dissolved.

5.1.3. Montmorillonite-to-zeolite conversion

The montmorillonite-to-zeolite conversion is frequently considered as a possible chemical transformation for bentonite barrier in the radioactive waste repository. For example, in the laboratory experiments (closed system at 300 °C), the zeolite group was identified (Guillaume, 2002). Evidently, 300 °C is far from the expected temperature. In the KIRMAT simulations (case 1–case 5), three tectosilicates were tested (see Table 2). The results show that only the Na-phillipsite precipitates, but this tectosilicate is not stable in the system because there is a

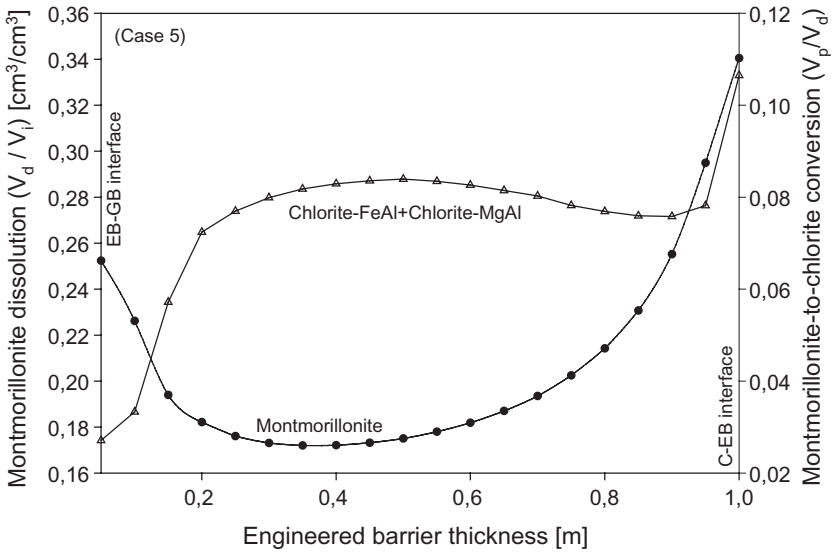

Fig. 6. Montmorillonite dissolution and montmorillonite-to-chlorite conversion for a bentonite barrier in the radioactive waste repository (case 5). V=Volume; i=initial and d=dissolved.

simultaneous dissolution of this mineral. In consequence, the montmorillonite-to-zeolite conversion under these conditions was not significant and/or considered as a transient phenomenon.

5.2. Final state of the bentonite barrier

Figs. 7–9 allow to compare the initial state with the final state of the engineered barrier after 1000 years of reaction and transport (cases 5, 6, and 7). The present study has shown that the Na/Ca–montmorillonite-to-Ca–montmorillonite conversion is the most significant chemical transformation, i.e., the chemical transformation from a medium-swelling clay to a low-swelling clay. In fact, this chemical process appears to be a simple cation exchange into the engineered barrier. This process only represents about 22% in the worst case (i.e., in both sides of engineered barrier, Figs. 7b,

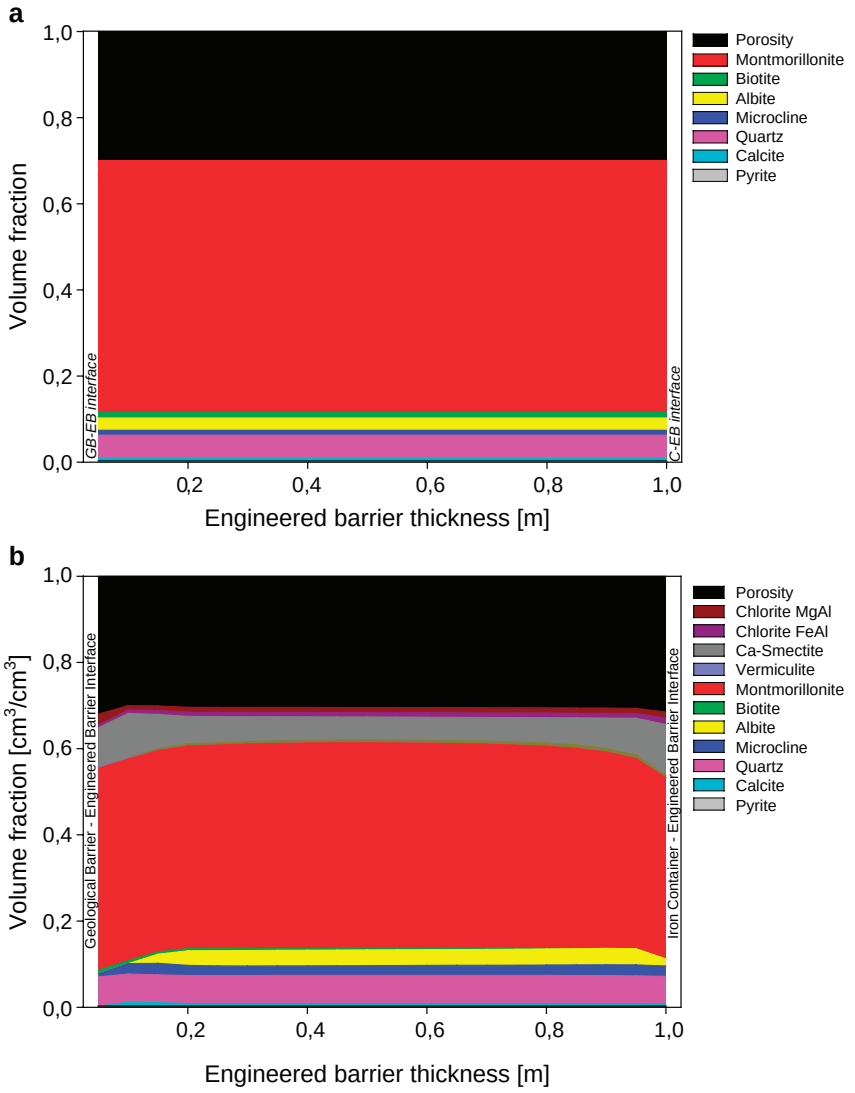

Fig. 7. (a) Initial state of the engineered barrier (case 5). Mineral composition (primary minerals) and porosity. (b) Final state of engineered barrier after 1000 years of reaction and transport (case 5). Mineral composition (primary minerals+secondary minerals) and porosity. This figure can be viewed in colour in the web version of this paper.

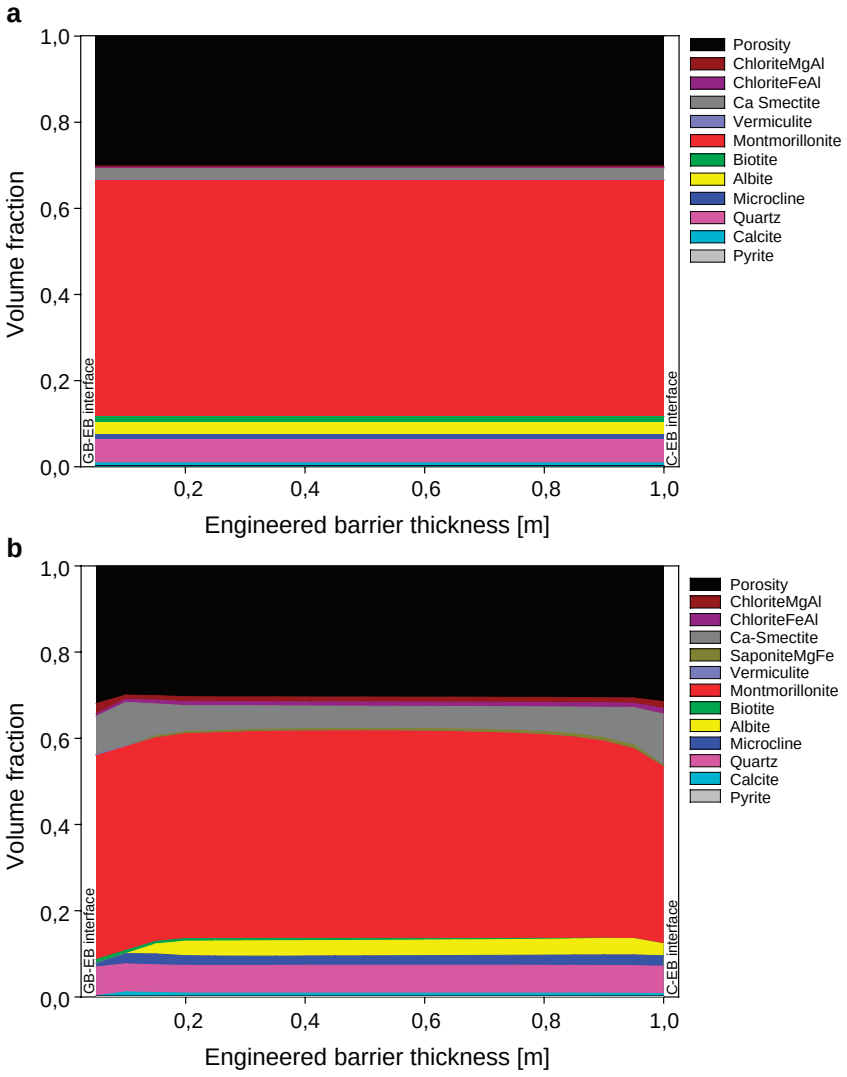

Fig. 8. (a) Initial state of the engineered barrier (case 6). Mineral composition (primary minerals) and porosity. (b) Final state of engineered barrier after 1000 years of reaction and transport (case 6). Mineral composition (primary minerals+secondary minerals) and porosity. This figure can be viewed in colour in the web version of this paper.

8b, and 9b). Here, the Ca–montmorillonite formation increases proportionally with the Na/Ca–montmorillonite transformation.

The initial physical porosity of the bentonite barrier (0.3 [L^{-3}/L^{-3}]) was also represented in Figs. 7–9. This physical property was slightly modified after 1000 years of reaction and transport (Fig. 7b, 8b, and 9b). In fact, a short increase was observed in both sides of the engineered barrier. Then, the porosity was kept similar to the initial value (0.29–0.30 [L^{-3}/L^{-3}]). It is important to mention that KIRMAT code considers the porosity variation as a function of rock volume balance in the system (e.g., Steefel and Lasaga, 1990; Carnahan, 1992), without specifying the type of porosity, i.e., it does not take into account the porous morphology, the connectivity, the pores size, etc.

Finally, it is important to remark that when the engineered barrier is initially in steady state with the interacting solution, the montmorillonite dissolution in the system is slightly inferior. In this study, the

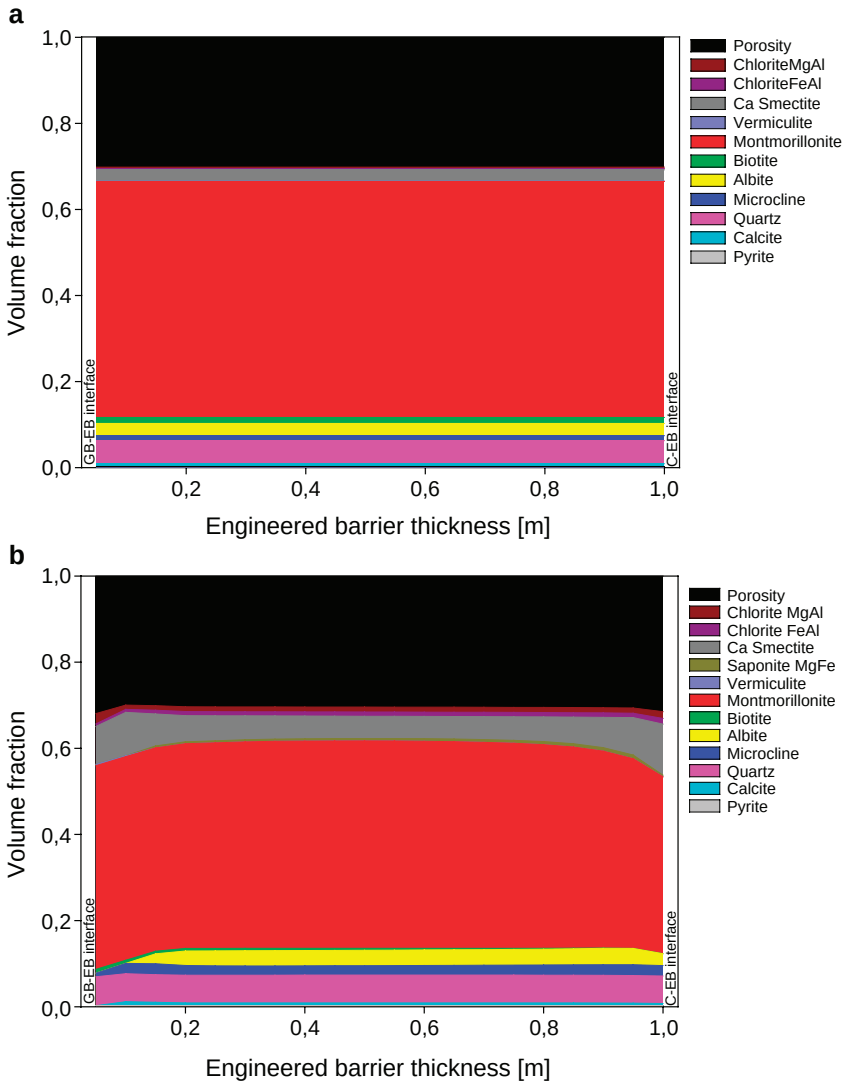

Fig. 9. (a) Initial state of the engineered barrier (case 7). Mineral composition (primary minerals) and porosity. (b) Final state of engineered barrier after 1000 years of reaction and transport (case 7). Mineral composition (primary minerals+secondary minerals) and porosity. This figure can be viewed in colour in the web version of this paper.

source type of iron in the boundaries of container shows a similar influence in the system.

5.3. Accessory minerals

The MX80 bentonite contains about 15% of accessory minerals (see Table 1). The nature and amount of these minerals in the system could limit or favour a chemical reaction. Sometimes, the accessory minerals could be inactive or slowly reactive. The final state of accessory minerals in the bentonite barrier after 1000 years of reaction and transport was not homogeneous (see Fig. 10). In fact, their dissolution/precipitation was always more significant in both sides of the engineered barrier, i.e., near the interfaces with the geological medium and with the iron container. Except for the pyrite, this was kept practically inactive in the system. The Fig. 10 also shows that the quartz, albite, and microcline precipitate in the engineered barrier while the calcite and biotite are partially dissolved.

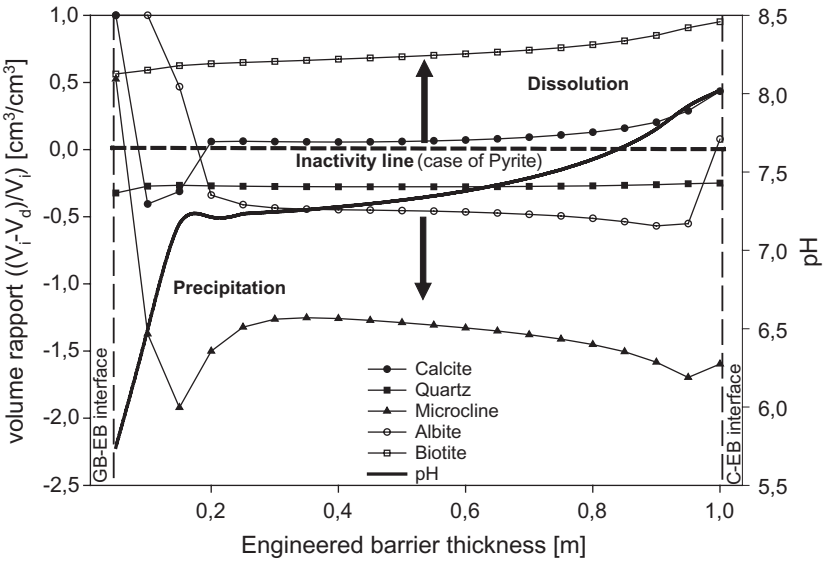

Fig. 10. Final state of accessory minerals of bentonite barrier after 1000 years of reaction and transport. V=Volume; i=initial and d=dissolved.

5.4. Chemical changes

5.4.1. pH and E_h evolution

The pH and E_h evolution for two different cases are shown in Fig. 11. A similar behaviour was observed for both cases. However, there is a significant parallel gap between E_h curves because of the initial state of the engineered barrier (in steady state with the chemical solution "case 6"or in disequilibrium with the chemical solution "case 5"). In general, the pH increases highly in the first 20 cm of engineered barrier. Generally, the pH increases slowly until a pH value slightly superior at 8. It is clear that there is a linear correlation between pH and oxidation–reduction potential (E_h) (Fig. 11). In fact, this correlation is inversely proportional, i.e., when the pH increases the oxidation–reduction potential decreases and vice versa. For example, the engineered barrier after 1000 years of reaction and transport presents the reducing properties more significant near of iron container ($E_h \cong -360$ mV).

5.4.2. Chemical-elements composition

High dissolution of the bentonite is manifested by the increased Si, Al, Mg, K, Ca, and Na contents in the interaction fluid.

The very low concentration in iron in the interaction fluid indicates chlorite precipitation in the system. This phenomenon is controlled by the silicate minerals dissolution and by the corrosion of iron container.

The insignificant variation in potassium content in the interaction fluid suggests that illitization was absent or insignificant.

5.5. Influence of diffusion coefficient

In order to evaluate the influence of diffusion coefficient on the montmorillonite dissolution, two values were tested in the KIRMAT simulations. Fig. 12 shows the montmorillonite volume fraction after 1000 years of reaction and transport. In general, the montmorillonite dissolution increases when the diffusion coefficient increases. For this study, the total increase of montmorillonite dissolution lies between 7% and 15% when the diffusion coefficient is changed from 10^{-11} to 10^{-10} m^2/s.

6. Conclusion

The chemical transformations occurring in a bentonite barrier for radioactive waste confinement depend directly on the reaction temperature, the rate of iron corrosion, the composition of interaction fluid, the nature and/or amount of accessory minerals, the

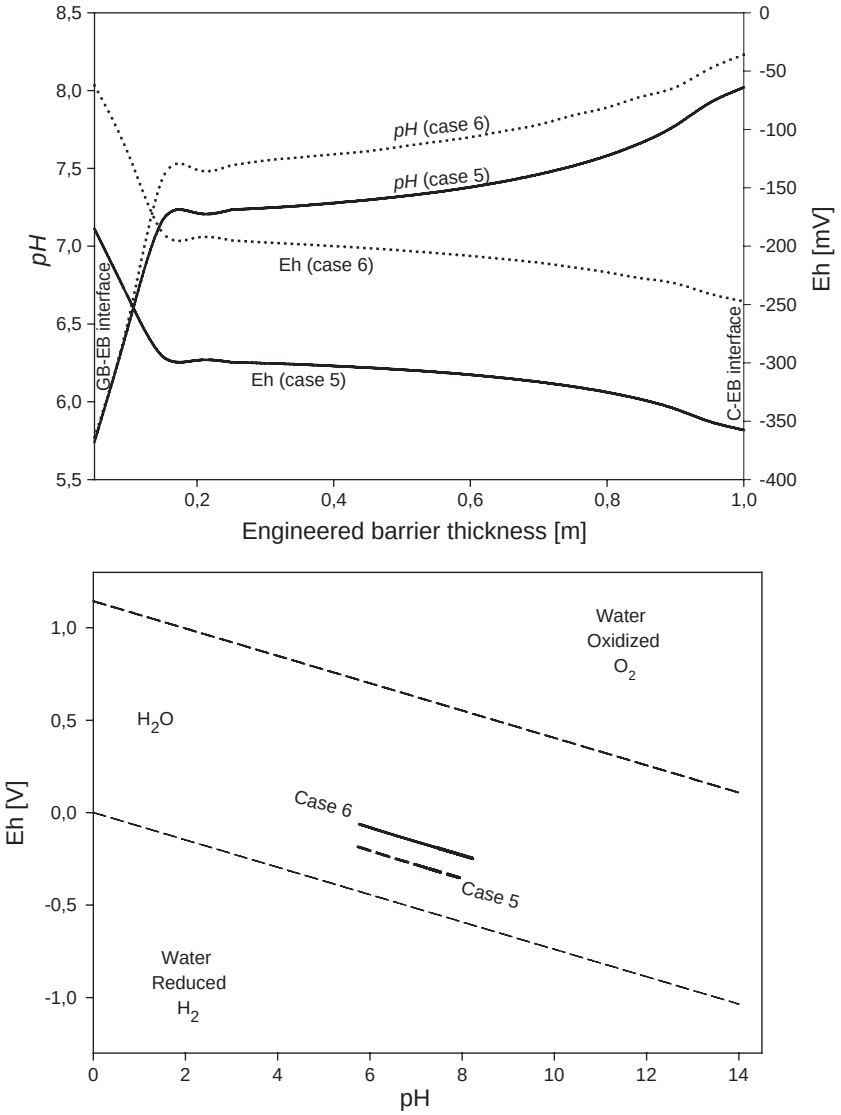

Fig. 11. pH and E_h evolution of interaction fluid after 1000 years of reaction and transport. (E_h=oxidation–reduction potential [mV]).

diffusion coefficients of solutes, the reactive surface area of minerals, the texture of porous media, etc. At the present time, it is difficult to efficiently consider all parameters in the same model because of the complexity of their estimation. Consequently, the KIRMAT simulations were carried out under drastic conditions of radioactive waste repository. The results show that Na/Ca–montmorillonite-to-Ca–montmorillonite conversion, the montmorillonite-to-chlorite conversion and dissolution/precipitation of accessory minerals were the most relevant chemical processes. The first chemical transformation represents about 22% in the worst case, i.e., near of the engineered barrier interfaces, while the second chemical transformation only represents about 3% (near the container), i.e., a high concentration of iron favours the chlorite–FeAl precipitation. Concerning the dissolution/precipitation of accessory minerals, in general, it

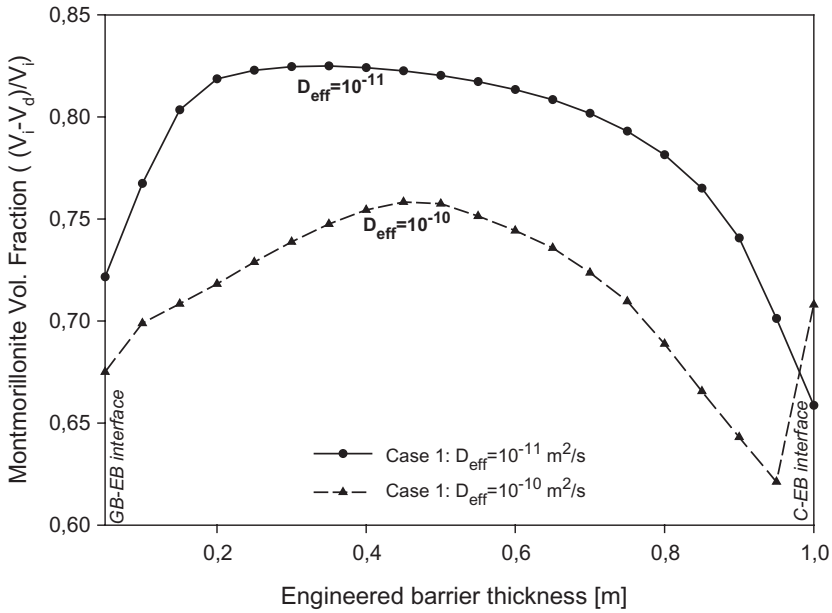

Fig. 12. Influence of diffusion coefficient on the montmorillonite dissolution after 1000 years of reaction and transport. V=Volume; i=initial and d=dissolved.

was observed that the quartz, microcline, and albite were re-precipitated in the system; the calcite and biotite were partially dissolved, and the pyrite kept inactive.

On the other hand, only a short augmentation of total porosity was observed near of engineered barrier interfaces.

Finally, it was also observed that the montmorillonite dissolution increases when the diffusion coefficient increases. Here, the total increase of montmorillonite dissolution lies between 7% and 15% when the diffusion coefficient is changed from 10^{-11} to 10^{-10} m^2/s.

The present indicative study suggests that the bentonite barrier could preserve its physical–chemical and mechanical properties after 1000 years of reaction and transport.

Acknowledgements

The authors are grateful to the French National Radioactive Waste Management Agency (ANDRA), in the framework of its program on the geochemical behaviour of bentonite engineered barrier, for providing a financial support for this work.

References

Bertrand, C., Fritz, B., Sureau, J.-F., 1994. Hydrothermal experiments and themo-kinetic modelling of water–sandstone interactions. Chem. Geol. 116, 189–202.

Carnahan, C.L., 1992. Numerical simulation of heterogeneous chemical reactions coupled to fluid flow in varying thermal field. Scientific Basis for Nuclear Waste Management XV. Mat. Res. Soc. Symp. Proc., vol. 257, pp. 683–690.

Chermak, J.A., Rimstidt, J.D., 1989. Estimating the thermodynamic properties (ΔG_f^0 and ΔH_f^0) of silicate minerals at 298 K from the sum of polyhedral contributions. Am. Mineral. 74, 1023–1031.

Chermak, J.A., Rimstidt, J.D., 1990. Estimating the free energy of formation of silicate minerals at high temperatures from the sum of polyhedral contributions. Am. Mineral. 75, 1376–1380.

Collin, F., Li, X.L., Radu, J.P., Chalier, R., 2002. Thermo-hydro-mechanical coupling in clay barriers. Eng. Geol., 64, 179–193.

Fritz, B., 1975. Etude themodynamique et simulation des reactions entre minéraux et solutions. Application à la géochimie des altérations et des eaux continetales. Mém. Sci. Géol., vol. 41. Strasbourg, France. 153 p.

Fritz, B., 1981. Etude thermodynamique et modélisation des réactions hydrothermales et diagénétiques. Mém. Sci. Géol. 65, 197.

Fritz, B., Tardy, Y., 1976. Séquence de minéraux secondaires dans l'altération des granites et roches basiques: modèles thermodynamiques. Bull. Soc. Géol. Fr. 18, 7–12.

Gens, A., Guimaraes, L., do, N., Garcia-Molina, A., Alonso, E.E., 2002. Factors controlling rock–clay buffer interaction in a radioactive waste repository. Eng. Geol. 64, 297–308.

Gérard, F., Clement, A., Fritz, B., 1998. Numerical validation of a Eulerian hydrochemical code using a 1D multisolute mass transport system involving heterogeneous kinetically controlled reactions. J. Contam. Hydrol. 30, 201–216.

Guillaume, D., 2002. Etude expérimentale du système fer-smectite en présence de solution à 80 °C et 300 °C. PhD Thesis, Henri Poincaré University, Nancy I, France. 210 p.

Helgeson, H.C., Brown, T.H., Nigrini, A., Jones, T.A., 1970. Calculations of mass transfer in geochemical processes involving aqueous solutions. Geochim. Cosmochim. Acta 34, 569–592.

Hökmark, H., 2004. Hydration of the bentonite buffer in a KBS-3 repository. Applied Clay Science 26, 219–233.

Hökmark, H., Karnland, O., Pusch, R., 1997. A technique for modeling transport/conversion processes applied to smectite-to-illite conversion in HLW buffers. Eng. Geol. 47, 367–378.

Jacquot, E., 2000. Modélisation thermodynamique et cinétique des réactions géochimiques entre fluides de bassin et socle cristallin. PhD Thesis, Louis Pasteur University, Strasbourg I, France. 202 p.

Jacquot, E., 2002. Composition des eaux interstitielles des argilites du Callovo-Oxfordien non perturbées. Rapport ANDRA No. D NT ASTR 02-041. 13p.

Kälvenius, G., Ekberg, C., 2003. TACK—a program coupling chemical kinetics with a two-dimensional transport model in geochemical systems. Comput. Geosci. 29, 511–521.

Keijzer, Th.J.S., Kleingeld, P.J., Loch, J.P.G., 1999. Chemical osmosis in compacted clayed material and the prediction of water transport. Eng. Geol. 53, 151–159.

Kluska, J.M., Fritz, B., 2001. Modélisation Thermodynamique et Cinétique des Réactions Géochimiques dans une Barrière Ouvragée en Bentonite. Simulations dans des conditions réductrices, de 60 à 180 °C en l'absence et en présence d'une source de fer sur une durée de 20 ans. Rapport ANDRA No. CRP 0CGS 01-004. 34p.

Le Gallo, Y., Bildtein, O., Brosse, E., 1998. Coupled reaction-flow modelling of diagenic changes in reservoir permeability, porosity and mineral compositions. J. Hydrol. 209, 366–388.

Lehikoinen, J., Carlsson, J., Muurinen, A., Olin, M., Salonen, P., 1996. Evaluation of factors affecting diffusion in compacted bentonite. Mat. Res. Soc. Symp. Proc. 412, 675–682.

Madé, B., Clément, A., Fritz, B., 1994. Modelling mineral/solution interactions: the thermodynamic and kinetic code KINDISP. Comput. Geosci. 20 (9), 1347–1363.

Malisis, M.A., Shackelford, C.D., 2002. Theory for reactive solute transport through clay membrane barriers. J. Contam. Hydrol. 59, 291–316.

Montes-H, G., 2002. Etude expérimentale de la sorption d'eau et du gonflement des argiles par microscopie électronique à balayage environnementale (ESEM) et analyse digitale d'images. PhD Thesis, Louis Pasteur University, Strasbourg I, France.

Montes-H, G., Duplay, J., Martinez, L., Mendoza, C., 2003. Swelling-shrinkage kinetics of MX80 bentonite. Appl. Clay Sci. 22, 279–293.

Montes-H, G., Duplay, J., Martinez, L., Escoffier, S., Rousset, D., 2004. Structural modifications of Callovo-Oxfordian argillite under hydration/dehydration conditions. Appl. Clay Sci. 25, 187–194.

Nagy, K.L., Cygan, R.T., Hanchar, J.M., Sturchio, N.C., 1999. Gibbsite growth kinetics on gibbsite, kaolinite, and muscovite: atomic force microscopy evidence for epitaxy and assessment of reactive surface area. Geochim. Cosmochim. Acta 63 (16), 2337–2351.

Neaman, A., Pelletier, M., Villieras, F., 2003. The effects of exchanged cations, compression, heating and hydration on textural properties of bulk bentonite and its corresponding purified montmorillonite. Appl. Clay Sci. 22, 153–168.

Nöack, Y., Collin, F., Nahon, D., Delvigne, J., Michaux, L., 1993. Secondary-mineral formation during natural weathering of pyroxene: review and thermodynamic approach. Am. J. Sci. 293, 111–134.

Poinssot, C., Toulhoat, P., 1998. Chemical interaction between a simulated nuclear waste glass and different backfill materials under a thermal gradient. Appl. Geochem. 13 (6), 715–734.

Sauzeat, E., Guillaume, D., Neaman, A., Dubessy, J., François, M., Pfeiffert, C., Pelletier, M., Ruch, R., Barres, O., Yvon, J., Villéras, F., Cathelineau, M., 2001. Caractérisation minéralogique, cristallochimique et texturale de l'argile MX80. Rapport ANDRA No. CRP0ENG 01-001. 82p.

Savage, D., Noy, D., Mihara, M., 2002. Modelling the interaction of bentonite with hyperalkaline fluids. Appl. Geochem. 17, 207–223.

Steefel, C.I., Lasaga, A.C., 1990. Permeability changes due to coupled flow and reaction. In: Melchior, D.C., Basset, R.L. (Eds.), Chemical Modelling of Aqueous Systems II, Am. Chem. Soc. Symp. Ser., vol. 416, pp. 212–216.

Tournassat, C., Neaman, A., Villiéras, F., Bosbach, D., Charlet, L., 2003. Nanomorphology of montmorillonite particles: estimation of the clay edge sorption site density by low pressure gas adsorption and AFM observations. Am. Mineral. 88, 1989–1995.

Ulm, F.J., Heukamp, F.H., Germaine, J.T., 2002. Residual design strength of cement-based materials for nuclear waste storage systems. Nucl. Eng. Des. 211, 51–60.

White, A.F., Peterson, M.L., 1990. Role of reactive-surface-area characterization in geochemical kinetic models. In: Melchior, D., Bassett, R. (Eds.), Chemicals Modelling of Aqueous Systems II, Assoc. Chem. Soc. Symp. Ser., vol. 416, pp. 461–475.